Cryo-Electron Microscopy and Three-Dimensional Reconstruction of the Calcium Release Channel/Ryanodine Receptor from Skeletal Muscle

Michael Radermacher,* Vibha Rao,*§ Robert Grassucci,* Joachim Frank,*‡ Anthony P. Timerman,‖ Sidney Fleischer,‖ and Terence Wagenknecht*‡

*Wadsworth Center for Laboratories and Research, New York State Department of Health, Albany, New York 12201-0509; ‡Department of Biomedical Sciences, School of Public Health, and §Department of Physics, State University of New York at Albany, Albany, New York 12222; and ‖Department of Molecular Biology, Vanderbilt University, Nashville, Tennessee 37235

Abstract. The calcium release channel (CRC) from skeletal muscle is an unusually large tetrameric ion channel of the sarcoplasmic reticulum, and it is a major component of the triad junction, the site of excitation contraction coupling. The three-dimensional architecture of the CRC was determined from a random conical tilt series of images extracted from electron micrographs of isolated detergent-solubilized channels prepared in a frozen-hydrated state. Three major classes of fourfold symmetric images were identified, and three-dimensional reconstructions were determined for two of these. The two independent reconstructions were almost identical, being related to each other by a 180° rotation about an axis in the plane of the specimen grid.

The CRC consists of a large cytoplasmic assembly (29 × 29 × 12 nm) and a smaller transmembrane assembly that protrudes 7 nm from one of its faces. A cylindrical low-density region, 2–3 nm in apparent diameter, extends down the center of the transmembrane assembly, and possibly corresponds to the transmembrane Ca^{2+}-conducting pathway. At its cytoplasmic end this channel-like feature appears to be plugged by a globular mass of density. The cytoplasmic assembly is apparently constructed from 10 or more domains that are loosely packed together such that greater than 50% of the volume enveloped by the assembly is occupied by solvent. The cytoplasmic assembly is suggestive of a scaffolding and seems well adapted to maintain the structural integrity of the triad junction while allowing ions to freely diffuse to and away from the transmembrane assembly.

In striated muscle the calcium release channel (CRC)[1], also known as the ryanodine receptor, plays a key role in excitation-contraction coupling, the process by which neuronal-induced depolarization of the sarcolemma leads to release of calcium from the lumen of the sarcoplasmic reticulum (SR). The CRC is an intracellular integral membrane protein of the SR (for reviews see Fleischer and Inui, 1989; McPherson and Campbell, 1993). Depolarization of the sarcolemma causes the CRC to open by mechanisms (apparently different in cardiac and skeletal muscle) whose elucidation represents the central remaining problem in understanding excitation-contraction coupling.

Several groups succeeded in purifying the CRC from skeletal muscle, and in reconstituting Ca^{2+} channel activity in lipid bilayers (Inui et al., 1987; Imagawa et al., 1987; Hymel et al., 1988; Smith et al., 1988; Lai et al., 1988). The channel was found to consist of a single polypeptide of unusually large mass, now known precisely from the sequence of the gene to be 565 kD (Takeshima et al., 1989; Zorzato et al., 1990). Electron microscopy (Inui et al., 1987; Saito et al., 1988; Lai et al., 1988; Wagenknecht et al., 1989; Radermacher et al., 1992) of the receptor showed an apparently fourfold symmetric complex having overall dimensions and morphology that matched those of the "foot" structure that had been observed previously in electron micrographs of sectioned muscle (Franzini-Armstrong, 1980; Franzini-Armstrong and Nunzi, 1983). Determination of the mass of the isolated CRC by quantitative scanning transmission electron microscopy confirmed the tetrameric nature of the channel (Saito, A., M. Inui, J. S. Wall, and S. Fleischer. 1989. Mass measurement of the feet structures/calcium release channel of sarcoplasmic reticulum by scanning transmission electron microscopy (STEM). *Biophys. J.* 55:206a.). Recent studies have shown that up to four copies of the immunophilin, FK-506 binding protein (M_r = 12 kD), are tightly associated with the channel after isolation, and it should be considered as an integral component of the CRC along with the 565-kD protein (Jayaraman et al., 1992; Timerman et al., 1993; Brillantes et al., 1994).

Please address all correspondence to Dr. M. Radermacher, Wadsworth Center for Laboratories and Research, New York State Department of Health, Albany, New York 12201-0509. Telephone: (518) 474-5821; FAX: (518) 474-7992.

1. *Abbreviations used in this paper*: CRC, calcium release channel; FRC, Fourier ring correlation criterion; POCS, projection onto convex sets; SR, sarcoplasmic reticulum.

The equivalence of the CRC and the foot structure is widely interpreted as indicating that the CRC has a central role in the signal transduction events of excitation-contraction coupling because foot structures are major components of the triad junctions, the sites where excitation-contraction occurs. At the triad junctions the sarcoplasmic reticulum and transverse tubules are held in close apposition, being separated by a gap of ~15 nm that is bridged by the foot structures. The transverse tubules are invaginations of the plasma membrane that allow changes in membrane polarization to be rapidly transmitted to the interior regions of muscle fibers. Dihydropyridine receptors (L-type calcium channels) are located in the transverse tubules and function as the voltage sensors in excitation-contraction coupling (for reviews see Numa et al., 1990; Rios et al., 1992). Electron microscopy and, more recently, biochemical studies strongly suggest a physical interaction between the dihydropyridine receptors and CRCs at the triad junctions (Block et al., 1988; Lu et al., 1994; Marty et al., 1994).

A key to understanding excitation-contraction coupling is to elucidate how the activity of the CRC is modulated by changes in the activity or conformation of the dihydropyridine receptor that occur in response to changes in transmembrane voltage. In skeletal muscle, a model is currently favored in which changes in the conformation of the dihydropyridine receptor are directly transmitted to the CRC (for reviews see Fleischer and Inui, 1989; Caswell and Brandt, 1989; Catterall, 1991; Rios and Pizzarro, 1991). To fully understand this process it is necessary to characterize the three-dimensional structures of the components and their structural relationships in the triad junction. As a first step in achieving this goal, we have focused on the isolated, solubilized CRC (Wagenknecht et al., 1989; Radermacher et al., 1992). In this report we describe three-dimensional reconstructions of the CRC determined from electron micrographs of frozen-hydrated specimens. The reconstructions are the most detailed yet obtained, revealing many new structural details.

Materials and Methods

CRCs were purified from terminal cisternae membrane fractions by ultracentrifugation through sucrose density gradients by a modification (Timerman et al., 1993) of the procedure described by Lai et al. (1988). The terminal cisternae were prepared from rabbit skeletal muscle as described by Saito et al. (1984).

Cryo-electron microscopy was done as described previously (Radermacher et al., 1992) with the following modifications. Molybdenum grids (300 mesh [Ted Pella, Inc., Redding, CA], coated with a thin carbon film supported by a thicker holey film), were used instead of copper grids because of their lower thermal expansion coefficient (Glaeser, 1992; Booy and Pawley, 1993). The solubilized CRC specimen was diluted to 0.025 mg/ml in buffer consisting of 20 mM Tris-HCl (pH 7.5), 0.5 M KCl, 2 mM DTT, 2 μg/ml leupeptin, 0.5% CHAPs. A 5-μl aliquot of specimen was applied to the grid for ~30 s, and then 2.5 μl was removed and replaced with 2.5 μl of H_2O to reduce the concentration of salts. Finally the grid was blotted from both sides and plunged into liquid ethane using a guillotine device modeled after that described by Cyrklaff et al. (1990). Each specimen area was imaged twice (magnification 38,000), first with the grid tilted by 50° and a second time without tilt.

Several hundred tilt/untilt pairs of micrographs were recorded and nine of these were selected for image processing. Micrographs of sufficient quality were routinely obtained for the untilted CRCs, but those of the tilted channels were usually not usable owing to specimen drift and charging artifacts. The micrographs were screened for these effects visually and by optical diffraction and only those that showed resolutions of better than 3 nm in all directions were used for further processing.

The three-dimensional reconstruction followed the method of Radermacher et al. (1987) (Radermacher, 1988) as implemented in the SPIDER software package (Frank et al., 1981*a*). Nine pairs of micrographs were digitized on a PDS 1010A flatbed scanning microdensitometer (Perkin-Elmer Corp., Norwalk, CT) using a 20-μm square aperture (corresponding to 0.526 nm on the specimen). A total of 1,665 pairs of CRC images were selected. The criteria used for this selection were that the CRCs should be clearly visible and separated from neighboring particles in both the tilted and untilted versions, and that they should appear in the fourfold symmetric orientation, the most common view. The images of untilted CRCs were translationally and rotationally aligned by correlation methods as in our earlier study (Radermacher et al., 1992). A fourfold symmetrized reference image was used for the alignment so as not to create an average that shows artificial asymmetric deviations from the fourfold symmetry of the CRC. If any significant deviations from this symmetry would have been present in the image set this should have become apparent in the image classification discussed below.

The aligned 0° images were submitted to correspondence analysis (van Heel and Frank, 1981; Frank and van Heel, 1982; Frank and Radermacher, 1992). Classification, using the dynamic clouds algorithm followed by hierarchical ascendant classification (Frank et al., 1988), was applied to the images based on the first eight factors of the correspondence analysis. Three classes of images were identified (see Results) and each was reanalyzed by correspondence analysis and classification to test for the presence of additional heterogeneity such as deviations from fourfold symmetry. No deviations from fourfold symmetry were detected at the current level of resolution (~3 nm).

For each of the three classes, average images were calculated and their resolutions determined using the 45° differential phase residual criterion (Frank et al., 1981*b*). Resolutions calculated from the Fourier ring correlation criterion (FRC) (Saxton and Baumeister, 1982; van Heel et al., 1982) are also stated where available. The phase residual criterion, which yields a more conservative estimate of the resolution (Unser et al., 1987; Radermacher, 1988) is used for all interpretations in this study.

Three-dimensional reconstructions were calculated separately for two of the three classes of images (classes II and III, see Results). The fourfold symmetry of the CRC was not enforced during the computation of the initial reconstructions but was used to determine their resolutions. For this purpose, each reconstruction was twofold symmetrized with respect to the fourfold symmetry axis, and then a phase residual analysis was performed in which the twofold symmetrized reconstruction was compared with itself after rotation by 90° about the fourfold axis. The phase residuals were computed along spherical shells in the three-dimensional Fourier transforms of the reconstructions. The reproducibility of the two independent reconstructions (from classes II and III) was also checked by a phase residual comparison between the two, after fourfold symmetrization.

The reconstructions were refined by application of the method of Projection onto Convex Sets (POCS, Youla and Webb, 1982; Sezan and Stark, 1982; Carazo and Carrascosa, 1987*a*,*b*; Carazo, 1992; Sezan, 1992). In a conical tilt series with a cone angle of 50°, as used in this study, a range of projecting directions, which all lie within a cone with opening angle 40° (=[90°-50°]) are undetermined. POCS makes use of certain a priori information (constraints) to partially correct the reconstructions for the effects of the missing cone of information. The particular implementation of POCS that was applied resembles the Gerchberg-Saxton algorithm (Gerchberg and Saxton, 1972) with the finite extent constraint (Gerchberg, 1974). It is the same procedure that had been used earlier for the reconstructions of ribosomal subunits (Radermacher, M., S. Srivastava, and J. Frank. 1992. The structure of the 50S ribosomal subunit from *E. coli* in frozen hydrated preparation reconstructed with SECRET. *Proc. 10th Europ. Congr. Electr. Micr.* 3:19–20). Briefly, the a priori information used is the stipulation that the volume surrounding the reconstruction should be featureless, because this part of the reconstruction is the result of averaging over the supporting carbon and vitreous ice in which the channels are embedded. Thus, any density modulations that occur outside of the CRC in a reconstructed volume are artifactual. A binary mask of dimensions known to be larger than those of the CRC was created from the reconstruction (Frank and Verschoor, 1984). The reconstruction was multiplied by this mask function in real space which changes all of the coefficients in Fourier space. The Fourier coefficients in the portion of the volume for which measured data were available, namely within the region outside the missing cone, were then replaced with their original (measured) values, and the reconstruction was transformed back to real space. This process was iterated until the reconstruction changed negligibly. Refinement by POCS resulted in no major changes in the reconstructions of frozen-hydrated CRCs, the main effect being an increase in the density of internal structural features, which gave the recon-

struction a more solid appearance. No new structural features were created when compared with the non-refined reconstructions.

Because we wished to compare our previous reconstruction of the negatively stained CRC (Wagenknecht et al., 1989), which had not been corrected using the POCS procedure, with the new reconstructions of frozen-hydrated CRC, we also applied POCS to the earlier reconstruction. After refinement, the reconstruction appeared more flattened than the unrefined one, an effect that was not seen with the reconstructions of ice-embedded CRCs (see Discussion).

Results

Cryo-Electron Microscopy

Nine pairs of electron micrographs (Fig. 1) were used to determine the three-dimensional reconstruction of the CRC. Two exposures were made for each specimen area, the first with the grid tilted by 50° and the second with the grid not tilted. The images of CRCs contained in the tilted micrograph were used for computing the three-dimensional reconstruction. From the nontilted specimen (Fig. 1 *b*), it is apparent that the CRCs adhere to the grid almost exclusively in an orientation in which their fourfold symmetry axes are perpendicular to the grid. This behavior has been documented previously (Radermacher et al., 1992).

Two-Dimensional Analysis

After their alignment, the images of untilted CRC were submitted to correspondence analysis and classification to characterize the heterogeneity present in the population of images and, if possible, to sort the images into homogeneous groups. The results of such an analysis, carried out on the 1,665 CRC images that were selected from the micrographs, indicated that there were three well-separated classes of images. This can already be seen in the correspondence analysis map of factor 1 vs factor 2 (Fig. 2). (For reviews on the use of correspondence analysis in image analysis see Frank, 1990; Frank and Radermacher, 1992). The three classes were approximately the same size: 502, 500, and 444 images in classes I, II, III, respectively.

Two-dimensional averages of the images from each set were computed (Fig. 3). The averaged images from groups II and III appear to be structurally identical except for a reversal of handedness, whereas the class I average does not have a clear handedness. The appearance of the class-II and -III images agrees with our previous studies of frozen-hydrated (Radermacher et al., 1992) and negatively stained CRCs (Saito et al., 1988; Wagenknecht et al., 1989). The mirror relationship between the class-II and class-III averages would be expected if the CRCs lie in two orientations on the specimen grid that are related by a 180° rotation about an axis in the plane of the grid (i.e., *right side up and upside down orientations*). The resolutions of the class II and III averages were similar, 2.7 (2.2) nm and 3.0 (2.3) nm, respectively. Here and in the following, we quote two values for the resolution, the first as determined by the 45° phase residual criterion and the second (in parentheses) by the Fourier ring-correlation method (see Materials and Methods).

The periphery of the images in class I does not allow for a differentiation of handedness, and the images comprising this class show a large degree of heterogeneity, which is reflected in the low resolution of their average, 3.7 (3.0) nm. At present we are unable to determine whether the channels in class I were structurally damaged, whether they were not as uniformly oriented on the grid as were the class II and III channels, or they were not precisely aligned during image processing. A combination of these factors is also quite possible. In any case, the class I images were not analyzed further.

Each class was subjected separately to correspondence

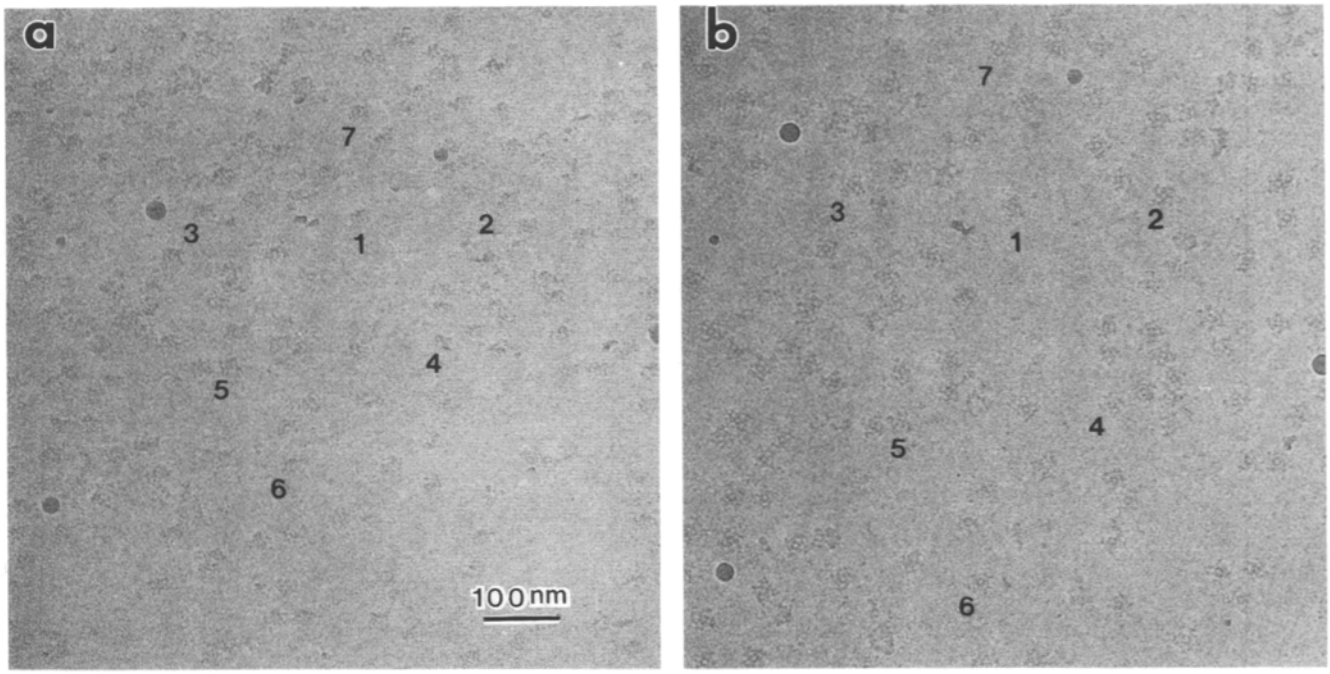

Figure 1. Cryo-electron microscopy of CRCs. (*a*) Portion of a micrograph recorded with the specimen grid tilted by 50°. (*b*) The same specimen field as in *a* except with the grid not tilted. A few of the same particles are labeled in both *a* and *b*.

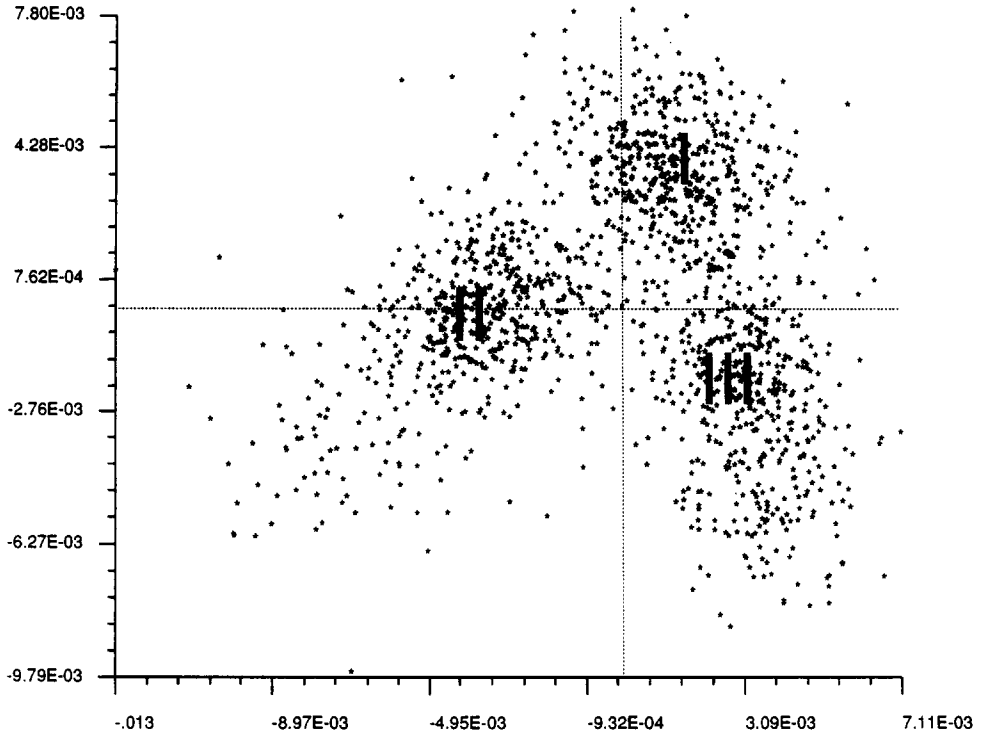

Figure 2. Separation of CRC images (*untilted*) into three classes by correspondence analysis. The map shows the coordinates of each image (*plotted as asterisks*) in a map of factor 1 (*abscissa*) vs factor 2 (*ordinate*). Even though classification has been applied to the images represented by factors 1-8, a separation into three classes can already clearly be observed in the projection onto the plane of factors 1 vs 2.

analysis to investigate any deviation from the fourfold symmetry. As in our earlier study (Radermacher et al., 1992), during the two-dimensional alignment of the particle set a fourfold symmetrized reference had been used so as not to enforce any artificial asymmetry. If the channel has only twofold symmetry, then correspondence analysis should have indicated the presence of two different populations. If no symmetry was present, then four groups should have been found. As in the earlier two-dimensional study no indication of a deviation from fourfold symmetry was found.

Three-Dimensional Reconstruction

Independent reconstructions were determined from the CRC images contained within classes II and III (Fig. 4). As we expected from the correspondence analysis of the untilted specimen images, in which classes II and III were identified, the reconstructions from the two classes were related by a 180° rotation, as if the channels lay on the specimen supporting film in right side up and upside down orientations.

The physical basis of this effect is not understood at present, and it was unexpected because in previous studies on negatively stained (Saito et al., 1988; Wagenknecht et al., 1989) or frozen-hydrated CRCs (Radermacher et al., 1992) we have not observed this behavior. The channels in our preparation are attached to a carbon film such that two different surfaces are formed, the air water and water carbon interfaces. It is unlikely that the channel would attach to both surfaces with equal probability. A more likely possibility is that, although the specimen was initially applied to only one side of the grid, the other side of the grid may also have been exposed to the specimen solution when the grid became sandwiched between filter paper during blotting.

As expected, neither the class II nor the class III reconstruction showed deviations from fourfold symmetry. From comparisons of corresponding sections from each of the two reconstructions, it is evident that the two reconstructions are very similar (Fig. 4). A phase residual analysis of the two reconstructions showed that they are reproducible to ~3.1 nm (Fig. 5). The reconstructions had resolutions of 3.3 nm (II) and 3.2 nm (III) as determined by a phase residual comparison of individual twofold averaged volumes with their 90° rotated versions (see Materials and Methods), and 3.1 nm in a comparison of both reconstructions with each other after fourfold symmetrization. Since they are nearly identical, the following description of the 3D architecture of the CRC will be illustrated by the fourfold symmetrized class-III reconstruction only. The relatively minor difference between the class II and III reconstructions will be treated below.

The three-dimensional architecture of the CRC is most easily comprehended from surface representations (Fig. 6). The volume represented by the surface views is 3,475 nm^3, which is equivalent to a molecular mass of 2,900 kD if a density of 1.37 g/cm^3 is assumed for the protein. This value of the molecular mass is in reasonable agreement with the mass of 2,300 kD predicted from the amino acid sequence of the CRC polypeptide (Takeshima et al., 1989; Zorzato et al., 1990) if allowance is made for the sensitivity of the mass estimate to the precise contour level chosen, for uncertainty (±2%) in the electron-optical magnification, and for an additional mass contributed by up to four molecules of tightly bound FK-506 binding protein (Timerman et al., 1993) and an unknown amount of detergent.

In agreement with our earlier reconstruction from a negatively stained specimen (Wagenknecht et al., 1989), the surface representations show that the CRC comprises two main structural components, a larger one having the shape of a square prism (29 × 29 × 12 nm) and, attached to one of its faces, a smaller protruding mass that in the previous negative stain reconstruction had been termed the "basal platform". This protruding mass is thought to contain the membrane-traversing segments of the CRC whereas the

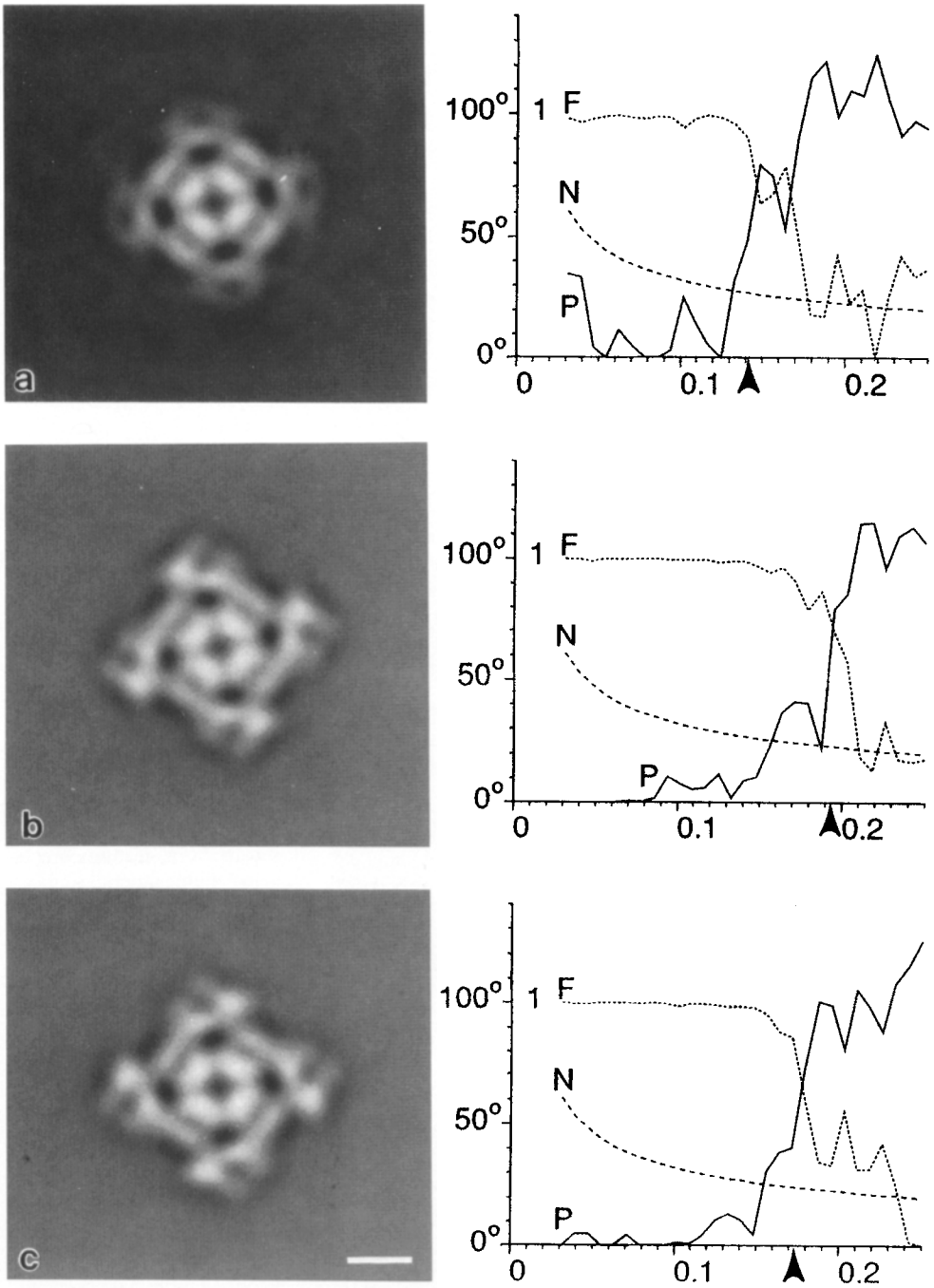

Figure 3. Averaged images of the CRC for each of the three classes identified by correspondence analysis. Contrast inverted relative to Fig. 1 such that presence of protein is shown in white. (*a*) class I, (*b*) class II, and (*c*) class III. Also shown with each average are phase residual (*P*) and Fourier ring-correlation curves (*F*). For the phase residual curves, the limiting resolution is defined by the Fourier spacing (*indicated by arrows*) at which the residual reaches 45°, whereas for the Fourier ring correlation the limiting resolution occurs where the curve crosses the curve (*N*) with twice the correlation value expected for noise, $2/\sqrt{N}$, *N* being the number of points used in the calculation. Vertical axis labeled 0°–100° for phase residual curve and from 0 to 1 for Fourier ring correlation curve. Abscissa in Fourier units of [(1/0.526) nm^{-1}]. Bar, 10 nm.

larger component projects into the myoplasm forming the so-called "foot structure" that has been observed in thin sections of skeletal muscle (Franzini-Armstrong, 1980); we will refer to the two structures as the transmembrane and cytoplasmic assemblies. Another convention that we will adopt is to refer to the surface of the reconstruction on the side bearing the transmembrane assembly as the sarcoplasmic surface. The opposite surface, which in situ would face away from the SR and towards the cytoplasm and transverse tubule, will be referred to as the cytoplasmic face. Supporting this assignment is the electron microscopy study of Ferguson et al. (1984) who showed by metal shadowing of heavy SR vesicles that the cytoplasmic surface of the foot structure (CRC) has a central depression similar to that observed in our three-dimensional reconstruction (Fig. 6 *a*).

The Transmembrane Assembly

The transmembrane assembly is depicted in Fig. 4 by sections *8–12*, and in the surface representations in Fig. 6, *b* and *c*. It is evident that this component is square-shaped in cross-section and tapered along the z-direction, having an edge length of 12 nm near the site of attachment to the cytoplasmic assembly and ~6 nm at its distal end. The total length of the transmembrane assembly along the z-direction, which would be normal to the SR membrane in situ, is 7 nm, more than sufficient to traverse a membrane bilayer.

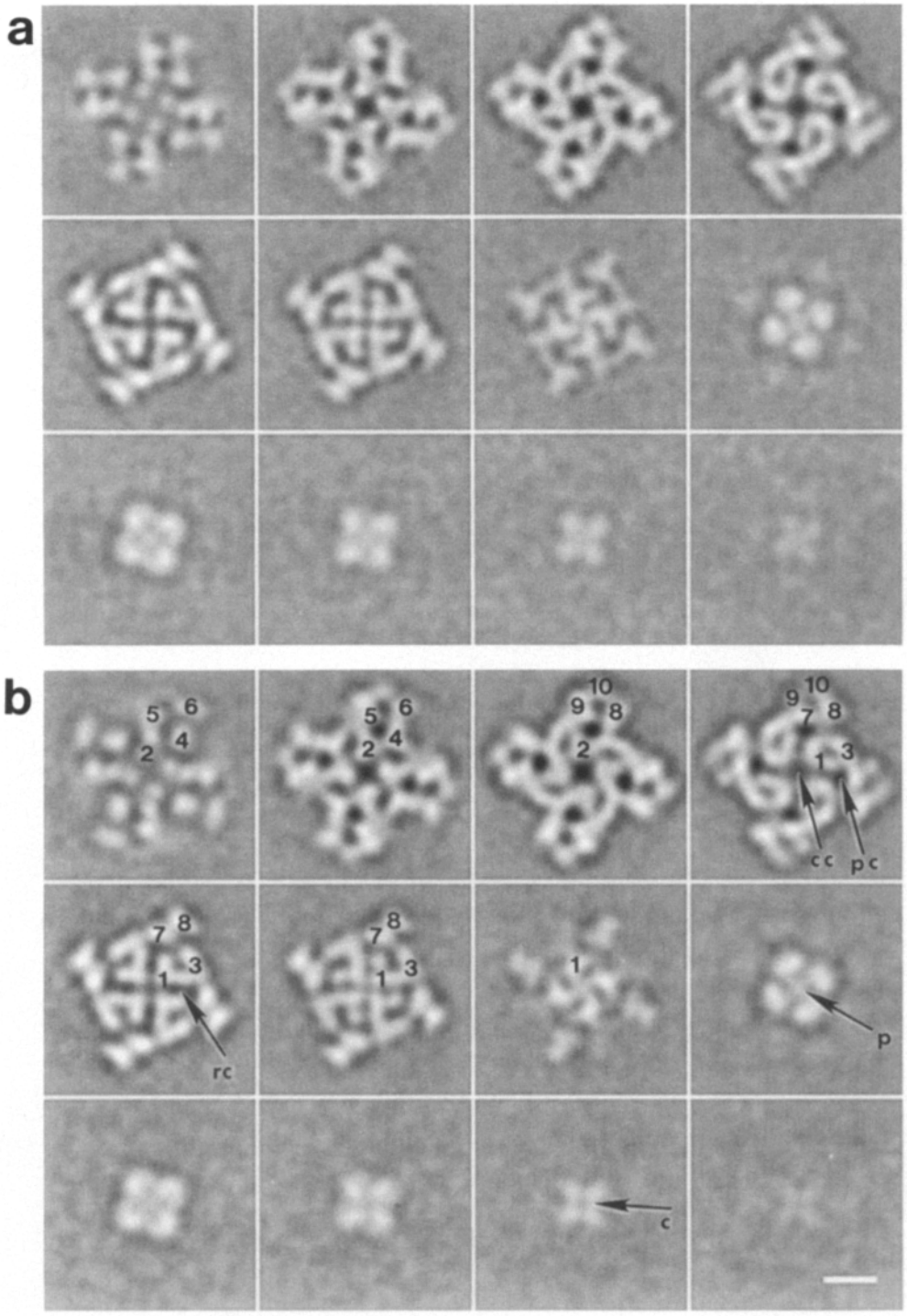

Figure 4. Selected z-slices spaced at 1.58-nm intervals (normal to fourfold symmetry axis, defined as the z-axis of the reconstruction) of the class-II (*a*) and class-III (*b*) three-dimensional reconstructions of the CRC. Some of the substructural features are labeled with numerals indicating to which domain they contribute (see text and Fig. 6 for description of the putative domain architecture). Other abbreviations: *c*, transmembrane low-density channel; *cc*, central cavity; *p*, plug feature; *pc*, major peripheral cavity; *rc*, radially running channels. Sections 1–7 (*counted from the upper left corner of the figure*) form the cytoplasmic assembly, sections 8–12 form the transmembrane assembly. Class III reconstruction has been rotated such that its orientation matches the one of the class II reconstruction. Bar, 10 nm.

A low-density channel of apparent diameter 2–3 nm appears to run down the center (i.e., along z) of the transmembrane assembly (see sections *9–12* in Fig. 4, *a* and *b*). Possibly this represents the path followed by Ca^{2+} in traversing the SR membrane. Intriguingly, in the z-sections nearest the cytoplasmic assembly (e.g., Fig. 4, *a* and *b*, section *9*), there appears to be a globular mass of density in the center of the channel that we will refer to as the "channel plug." The channel plug is also clearly resolved in surface representations of the channel that have been sliced in half along a direction parallel to z to reveal internal structural features (Fig. 7 *a*). The apparent diameter of the plug is 3.0–3.5 nm. At the contour level chosen to represent the CRC in Fig. 6, the plug is surrounded by four small cavities that lead to the exterior of the transmembrane assembly. One of these cavities is visible in Fig. 6 *c* just to the left of the label, "TA," and all four cavities are visible in Fig. 7 *c* (*middle*) between and just below the "1" domains of the cytoplasmic assembly.

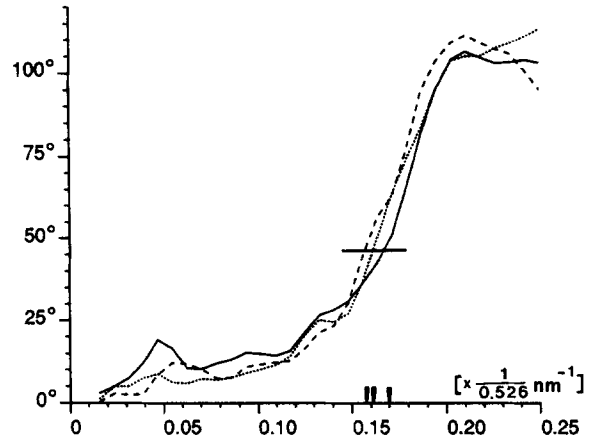

Figure 5. Phase residual curves obtained by comparison of twofold symmetrized reconstructions, calculated over shells in the three-dimensional Fourier transform of the volumes. Only the part of the volume measured by projections was used in this calculation. Sections that correspond to the missing cone were ignored. (*Large dashes*) reconstruction II; (*short dashes*) reconstruction III; (*solid line*) phase residual between fourfold symmetrized reconstructions II and III. Arrows on the x-axis indicate the 45° resolution limits.

The Cytoplasmic Assembly

Perhaps the most striking feature of the cytoplasmic assembly is the large fraction of its volume, estimated to be greater than 50%, that appears to be occupied by solvent (this is especially apparent in the view of the cytoplasmic face shown

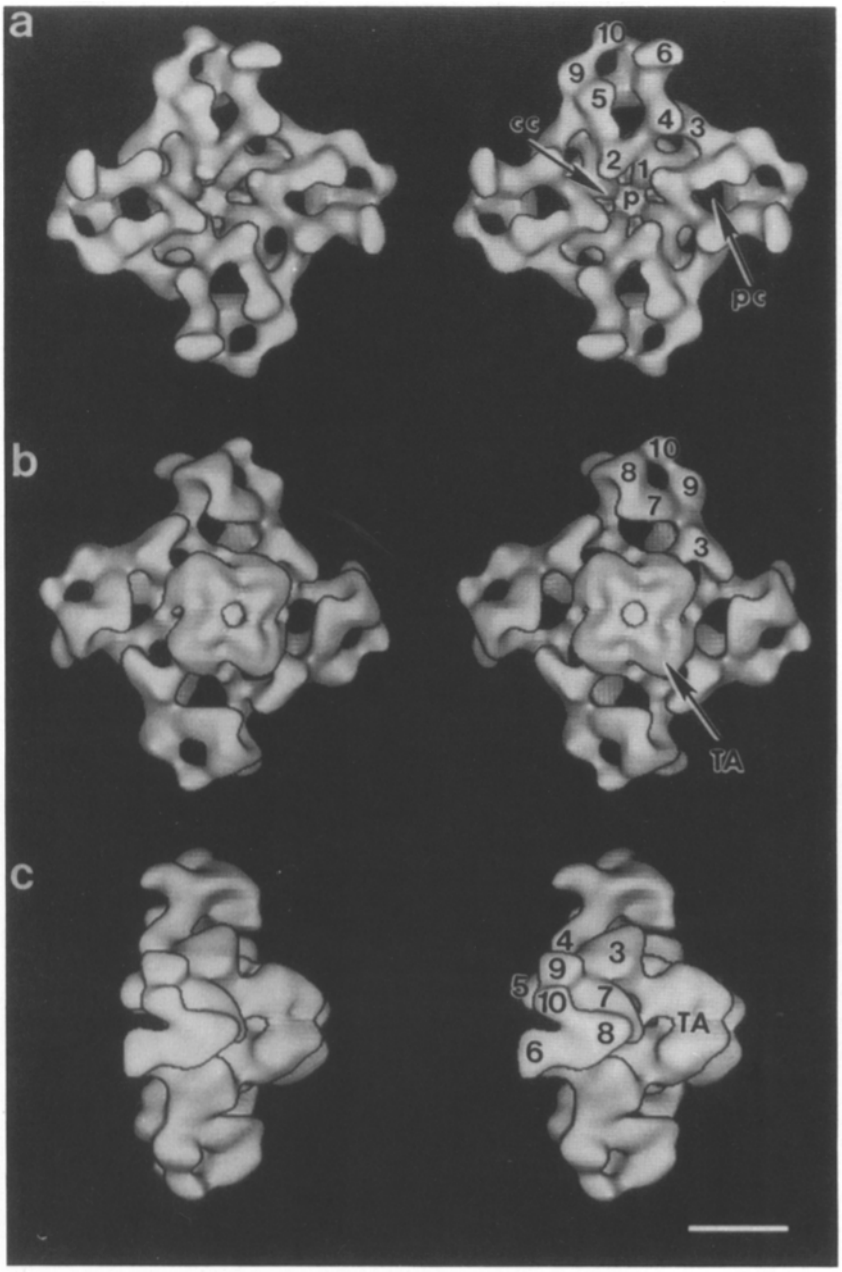

Figure 6. Surface representations (*stereo pairs*) of the class-III reconstruction. (*a*) View along fourfold symmetry axis showing the surface that would face the cytoplasm and the apposing transverse tubule in a triad junction. (*b*) View along fourfold axis onto the face that would interact with the sarcoplasmic reticulum. (*c*) Side view (*normal to fourfold axis*). One of the corners of the cytoplasmic assembly is near the center in the orientation shown. The putative structural domains are labeled with numerals. Other abbreviations are as defined in Fig. 4. Bar, 10 nm.

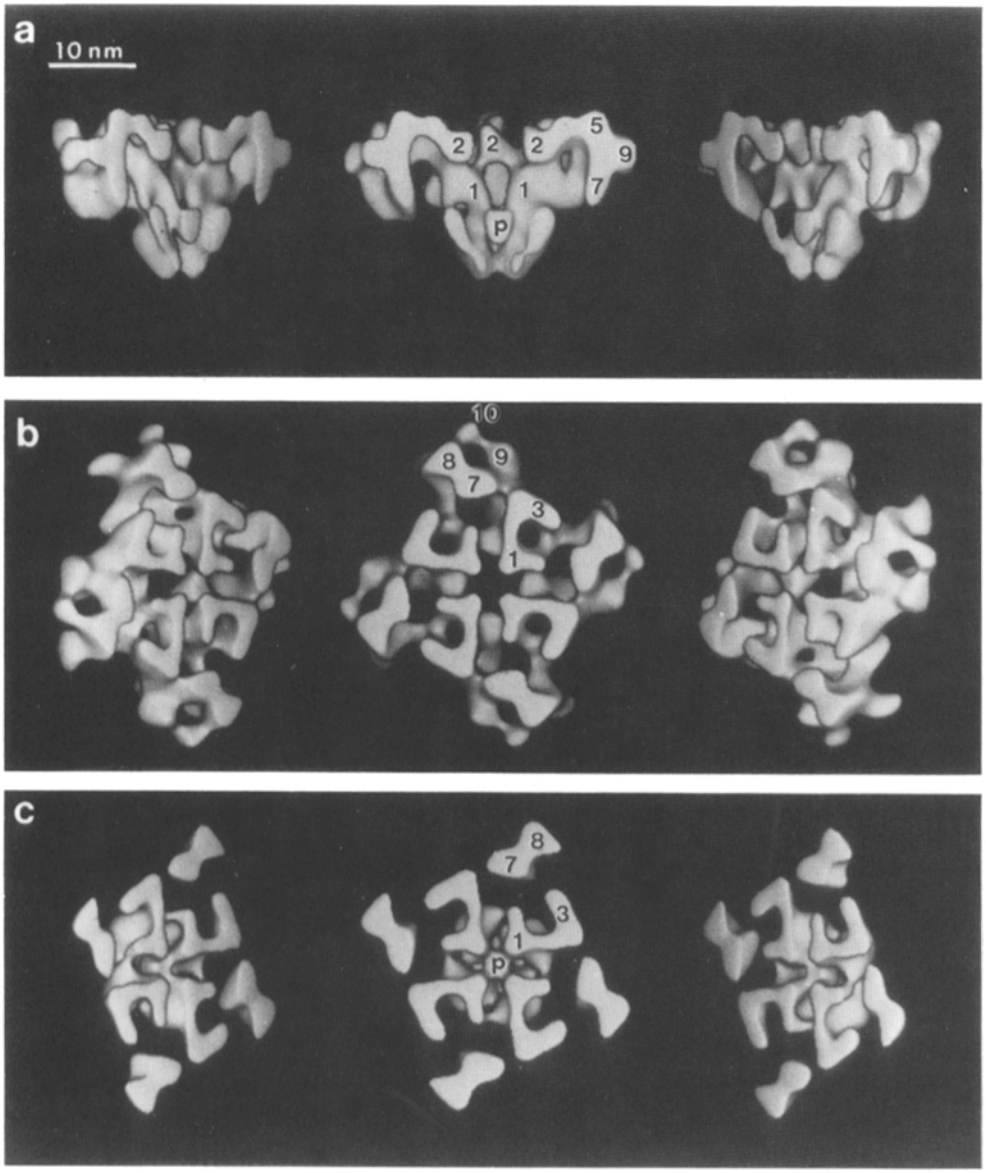

Figure 7. Internal structure of the CRC. The three-dimensional reconstruction determined from the class-III images was cut in half along two orthogonal directions and displayed as surface representations. (*a*) Three related views of the reconstruction cut parallel to the z-direction and along a diagonal of the cytoplasmic assembly. (*b*) Three views of the reconstruction cut perpendicular to the fourfold symmetry axis. The central image is a view from the cutting plane toward the cytoplasmic face. (*c*) Three views of the reconstruction sliced as in *b* and viewed from the cutting plane toward the face containing the transmembrane assembly. The views at the left and right in *a*, *b*, and *c* are related to the central one by +30° and −30° rotations about a vertical axis.

in Fig. 6 *a* when viewed in stereo). The four large solvent-filled cavities that are labeled "pc" in Fig. 6 were resolved in our earlier reconstruction of the CRC in negative stain, but a number of additional small internal cavities, pockets, and channel-like features are resolved in the new reconstructions.

The protein that forms the cytoplasmic assembly appears to be arranged as domains that are loosely packed together. We have tentatively identified 10 such domains and assigned numerals to them as indicated in Figs. 4, 6, and 7. The domains were identified on the basis of their distinctive globular shapes, but the precise locations of boundaries between adjacent domains are sometimes not well defined. Each of the 10 domains is, of course, repeated four times in the reconstruction of the tetrameric CRC, but we cannot determine, at the current resolution, how to apportion the domains to the subunits. Specifically, the domains to which we have assigned numerals in Fig. 4 should not be interpreted as forming one of the four subunits. When higher resolutions are achieved it might become apparent that some of the putative domains are themselves multidomain structures, or that some adjacent domains that are not so distinctly separated (e.g., domains *7* and *8*) are actually asymmetric single domains.

The topological relationships among the domains forming the cytoplasmic assembly can be discerned most clearly from the stereo surface representations shown in Fig. 6. Beginning at the center of the structure, domain 1 forms the only visible connections to the transmembrane assembly.

These arch-like domains bifurcate as they rise from the top surface of the transmembrane assembly to form connections with domains 2 and 3. In cross-section (perpendicular to z-axis) domain 1 appears roughly Y-shaped (Fig. 7 *b*, see also Fig. 4, sections *5* and *6*) with the two arms of the "Y" interacting with domains 2 and 3. The regions between the four copies of domain 1 form a striking cross pattern that corresponds to the radially running channels also observed in our earlier reconstruction (Wagenknecht et al., 1989).

Domains 4–10 form the large lobes that occupy the corners of the cytoplasmic assembly. The large peripheral cavities

(labeled *pc* in Figs. 4 and 6) are formed principally by domains 2, 4, 5, 6, and 7. Domain 10, the smallest (~3 nm in diameter) and most peripherally located domain, was not resolved in our earlier reconstruction and its presence accounts for the slightly larger x-y dimensions found for the cytoplasmic assembly in the new reconstructions (29 × 29 nm compared to 27 × 27 nm reported previously).

Comparison of Class-II and Class-III Reconstructions

As described above, the class-II and class-III reconstructions arose because the CRCs occurred in "right side up" and "upside down" orientations on the specimen grid. The largest difference between the two occurs in the cytoplasmic assembly in the vicinity of domains 5 and 6 on the cytoplasmic face (Fig. 8 *a*). In the class-III reconstructions, these two domains are separated by a deep cleft, whereas in the class-II reconstruction the cleft appears filled in with density and domain 6 appears smaller. It is not known whether this structural difference causes the CRCs to occur in the two orientations characterizing the class-II and class-III images, or whether it is an artifactual consequence of the two orientations. Several other minor differences between the two reconstructions, such as a slightly better contrasted central channel at the distal end of the transmembrane assembly for the class-III reconstruction (sections *11* and *12* in Fig. 4, *a* and *b* and Fig. 8 *b*), are not regarded as being significant.

Discussion

Comparison with Previous Results

The three-dimensional reconstructions that we have described for the skeletal muscle CRC contain many more structural details than were present in our previous reconstruction determined from negatively stained channels (Wagenknecht et al., 1989). The improvement is due mostly to the cryo-methodology that was used in the preparation and imaging of the channels. Excellent preservation of macromolecular ultrastructure, sometimes to near-atomic resolutions, has been described for frozen-hydrated macromolecules (see Chiu [1993] for a recent review of the technology).

The resolution-limiting factor in studies, such as this one, of noncrystalline macromolecular assemblies, is probably the defocusing of the microscope's objective lens. In a micrograph of a tilted specimen, the focus varies perpendicular to the tilt axis. With a tilt angle of 50° and a magnification of ~36,000 as used here, the range of defocus is ~2.5 μm such that in parts of the image the first zero of the transfer function limits the resolution to ~3 nm (for a review and introduction to the nature and effects of the contrast transfer function in cryo-electron microscopy see e.g., Stewart and Vigers, 1986).

The resolution of the three-dimensional reconstructions described here for the frozen-hydrated CRC is 3.1 nm, which is close to the limit expected for the degree of underfocus used. A first step for achieving higher resolution would be the use of spot-scanning (Downing and Glaeser, 1986) with dynamic focus adjustment as the beam travels perpendicular to the tilt axis (Zemlin, 1989), a technique that we hope to explore in the near future.

A well-known limitation of negative staining is that the dehydration of the specimen that occurs with this technique is often accompanied by a partial collapse or flattening of macromolecules against the carbon film support. Essentially all

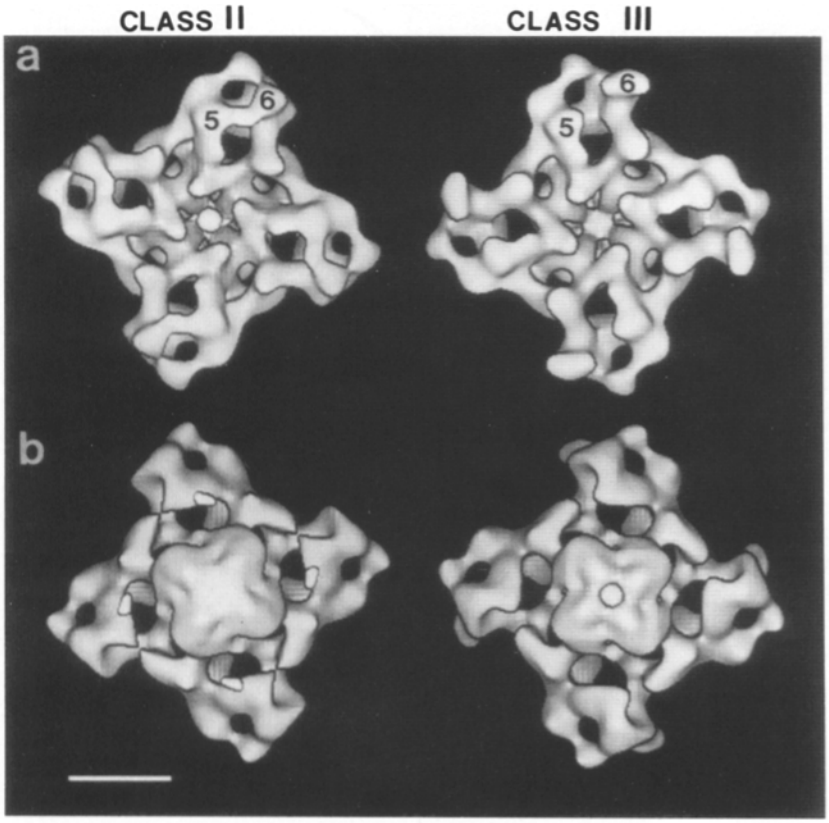

Figure 8. Comparison of reconstructions from class-II and class-III CRC images. (*a*) Surface representations showing the cytoplasmic face. (*b*) Surface representations showing the sarcoplasmic surface. In both *a* and *b* the class-II reconstruction is on the left and the class-III reconstruction on the right. Note the difference between the two in the region of domains 5 and 6 in *a*. As can be verified by a comparison with Fig. 4, the presence and absence of the central hole in *b* is due to minor differences in density, overemphasized by the effect of thresholding for surface representation. Bar, 10 nm.

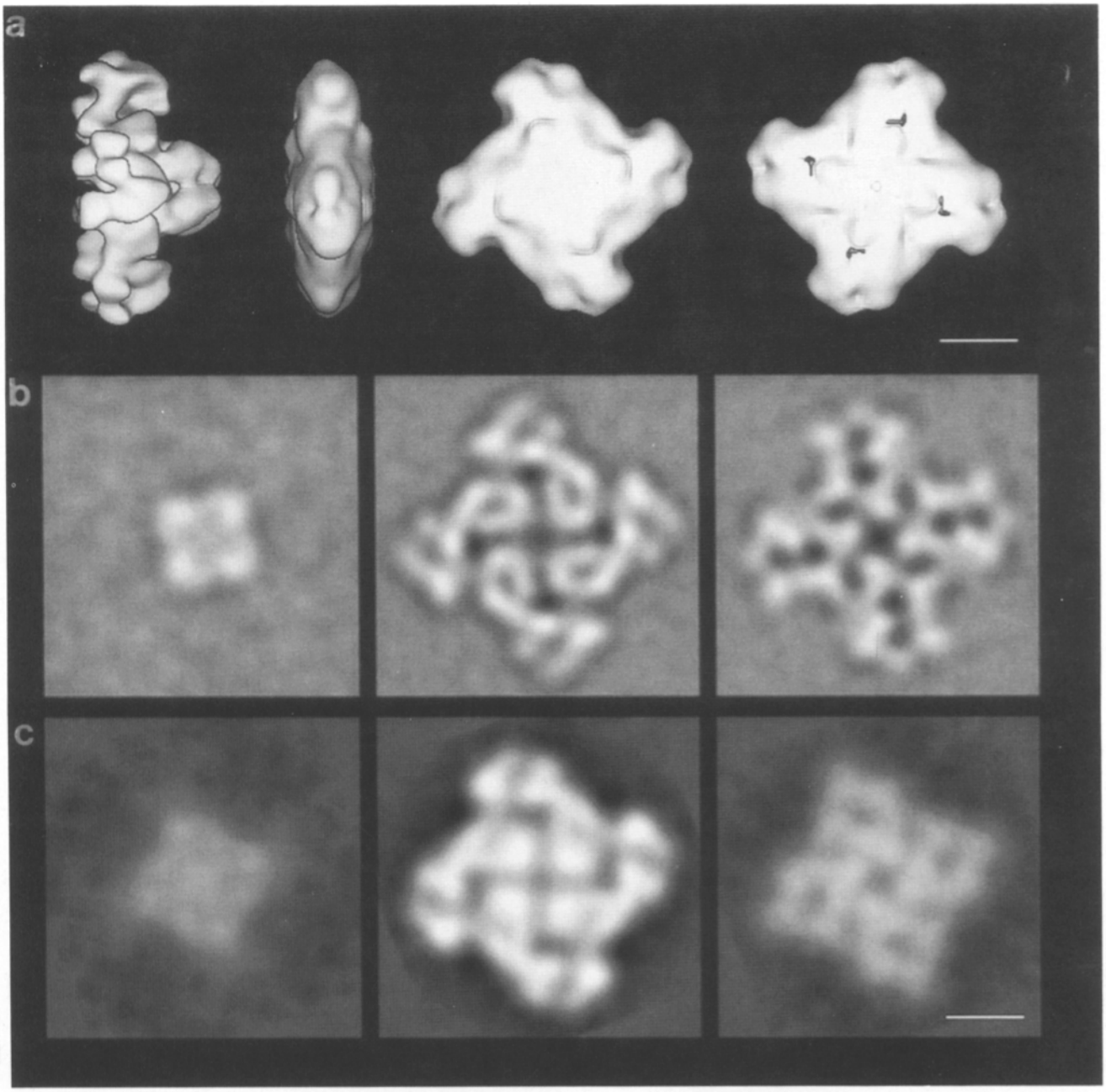

Figure 9. Comparison of three-dimensional reconstructions determined from negatively stained and frozen-hydrated CRCs. (*a*) Surface representations of frozen-hydrated (*leftmost image*) and negatively stained (*second image*) CRC in the side view. Views of the negatively stained CRC in SR- and cytoplasmic-facing views are shown in the third and fourth images from the left. The reconstruction from negatively stained specimen is from Wagenknecht et al. (1989) but has been refined with POCS (see Materials and Methods). (*b* and *c*) z-sections at selected levels from reconstructions of negatively stained (*c*) and frozen-hydrated (*b*) CRC. The three sections are at comparable z-coordinates in the two reconstructions.

of the differences between our previous reconstruction and the new ones can be attributed to the distortions and loss of resolution caused by dehydration of the negatively stained specimen. The flattening effect is readily apparent in side views (normal to the z-axis) of the reconstructions which show the maximal dimension in the z-direction to be 19 nm for the frozen-hydrated CRC and just 12 nm for the negatively stained CRC[2] (Fig. 9 *a*). Much of the flattening of the

2. Application of POCS to the reconstructed negatively stained CRC resulted in a significant reduction in the dimensions of the CRC in the z-direction, but no such effect was found when POCS was applied to the reconstructions of frozen-hydrated CRC. Similar behavior has also been found for the 50 S ribosomal subunit (Radermacher, M., S. Srivastava, J. Frank. 1992. The structure of the 50 S ribosomal subunit from *E. coli* in frozen hydrated preparation reconstructed with SECRET. *Proc. 10th Europ. Congr. Electr. Micr.* 3:19–20). It seems that reconstructions of negatively stained specimens behave more like "binary" objects, i.e., the main contributor to density differences is the presence or absence of stain. In these cases, one effect of the missing cone is an elongation of the object as a whole. In contrast, frozen-hydrated specimens behave as if they are constructed by superposition of elongated image points where the effect of the missing cone would mainly be to reduce the resolution in the z-direction rather than to elongate the entire object.

negatively stained CRC occurred in the transmembrane assembly, which projects less than 3 nm from the surface of the cytoplasmic assembly as compared with 7 nm for the frozen-hydrated CRC. Also, the transmembrane assembly appears to have collapsed onto the cytoplasmic assembly so that the connections between the two, formed by domain 1 in the frozen-hydrated reconstructions (Figs. 6 and 7), are not visible.

The transmembrane assembly in the reconstruction of the negatively stained CRC also appears rotated by ~40° about the z-axis relative to its orientation in the new reconstructions. Possibly, this, too, occurs during the drying of the specimen. The orientation of the transmembrane assembly relative to the cytoplasmic assembly in the newest reconstructions agrees well with the orientation proposed by Block et al. (1988) based on analysis of micrographs of freeze-dried, metal-shadowed CRCs.

Within the cytoplasmic domain, the major effect of drying on the reconstruction of negatively stained CRC is that the multi-domain architecture of the CRC seen in the new reconstructions is not apparent, as if the domains were pushed together and, consequently, no longer resolvable as the CRC became flattened. Also, the central cavity in the map from the negatively stained CRC does not extend all the way to the top of the cytoplasmic assembly as it does in the map of the frozen-hydrated CRC (compare Fig. 6 *a* with *rightmost image* Fig. 9 *a*).

Despite the flattening undergone by the negatively stained CRC, the main structural features seen in its three-dimensional reconstruction are also present in the new reconstructions. In the cytoplasmic assembly these features include the large peripheral cavities and the radial channels connecting them to the central cavity, and the large lobes at the corners of the assembly (Fig. 9, *b* and *c*). Thus the reconstruction obtained from negatively stained CRCs appears to be a somewhat lower resolution (3.7 nm), but mainly flattened representation of the three-dimensional architecture of the CRC as determined using cryo-methods.

The Transmembrane Assembly

Two lines of evidence support the interpretation that the structure we have termed the transmembrane assembly does indeed traverse the SR membrane bilayer. First, side views of negatively stained and frozen-hydrated solubilized CRCs have been observed by electron microscopy in which this assembly is clearly visible projecting off of one side of the CRC, whereas in side views of CRC's in isolated terminal cisternae vesicles this structure is not visible (Saito et al., 1988; our unpublished observations), suggesting that it is embedded in the bilayer where it cannot be resolved. Second, freeze-fracture electron microscopy of junctional SR membranes show a structure embedded in the membranes that corresponds in size and shape to the CRC transmembrane assembly (Block et al., 1988). The length of the transmembrane assembly as viewed from the side (Fig. 6 *c*) is 7 nm, which is several nanometers more than necessary to traverse the bilayer, and so possibly the distal portions of the assembly extend into the lumen of the SR.

Four cavities appear on the sides of the transmembrane assembly near its junction with the cytoplasmic assembly, and they extend to the channel plug (see Figs. 6 *c* and 7 *c* [*middle*]). Possibly these side cavities represent the main exit site to the myoplasm for calcium ions when the CRC is in its open state, in which case the cytoplasmic assembly need not be directly involved in the actual release of ions as we hypothesized previously (Wagenknecht et al., 1989). The transmembrane assembly extends distally 5 nm from the side openings which is still sufficient to span a membrane bilayer.

Multidomain Architecture of the Cytoplasmic Assembly

The three-dimensional structure of the CRC is unusual in that, despite the large size of its constituent subunit, 565 kD, it is a rather compact structure, unlike many other large polypeptides which are extended (e.g., the spectrin family [Speicher and Ursitti, 1994]). Our three-dimensional reconstructions show the CRC as being constructed from many domains. However, unlike the extended arrangement found for some other large polypeptides, the domains of the CRC appear to have undergone a kind of supra-tertiary folding in which a number of interdomain contacts are made such that the observed three-dimensional architecture is formed.

Despite forming a compact assemblage, the 10 tentatively identified domains (Fig. 6) contributed by each of the four subunits to the cytoplasmic assembly of the CRC are loosely packed together. We estimate that over 50% of the volume enclosed by the cytoplasmic assembly is accessible by solvent. We believe, for the following reasons, that the loose packing of the domains reflects the native architecture of the CRC as opposed to being induced somehow by the isolation procedure. First, the image averaging inherent in our reconstruction procedure will only resolve structural details that are conserved among the particles, and it is unlikely that denatured or damaged CRCs would have a conserved structure. Second, the isolated CRC still binds ligands, such as ryanodine, FK-506 binding protein (Timerman et al., 1993), and calmodulin (Wagenknecht et al., 1994), which associate with the native channel, indicating that native structure is retained in the isolated complex. Third, that such a large fraction of the CRC is occupied by solvent should have been evident even before the reconstruction was determined, because a simple calculation of the channel's volume from the exterior dimensions of the foot structures seen in electron micrographs of muscle or heavy SR vesicles (e.g., Ferguson et al., 1984; Saito et al., 1984) yields values that are 2–3 times greater than the volume expected for an assembly constructed from four 565-kD subunits.

The Cytoplasmic Domain as a Scaffolding

One of the roles of the cytoplasmic assembly is probably a mechanical one: to hold the transverse tubule and SR membrane systems in close proximity at the triad junction, and to maintain the junction during the potentially disruptive forces generated during cycles of muscle contraction. In performing this function, the cytoplasmic assembly must not impede substantially the dispersal of Ca^{2+} into the myoplasm when the CRC enters the open state. The cytoplasmic assembly appears well designed to perform this function. The loosely packed assemblage of structural domains comprising this structure and the complex pattern of interactions among them are reminiscent of a scaffolding designed to maintain structural integrity under stress. If calcium ions enter the cytoplasmic assembly upon emerging from the transmembrane assembly, then they would appear to have access

to a number of pathways to reach the myoplasm. Although the top surface of the cytoplasmic domain is open at its center, in the triad junction it may be blocked, and one of the major exit pathways for Ca^{2+} would be through the spaces between the domains labeled "1". These spaces appear as radially running channels in cross-section (Figs. 4 [section 5] and 7 *b*) and were also present in our previous reconstruction (Wagenknecht et al., 1989).

Potential Interaction with the Transverse Tubule

At a triad junction, the cytoplasmic surface of the CRC would interact with the transverse tubule. Recent studies argue for a direct interaction of the CRC with the voltage sensing dihydropyridine receptor (Lu et al., 1994; Marty et al., 1994), but the participation of accessory proteins, such as triadin, cannot be excluded (Caswell et al., 1991). Block et al. (1988) have obtained evidence from electron microscopy that every other CRC interacts with a cluster of four transverse tubule proteins (tetrads), thought to be dihydropyridine receptors. In their model of the triad, the four dihydropyridine receptors are located directly across from the four lobes of the CRC with which they interact, such that their centers define a square of edge length 13–14 nm.

In our three-dimensional reconstructions the cytoplasmic face of the cytoplasmic assembly is formed principally by three domains: 4, 5, and 6 in our designation (Fig. 6, *a* and *c*). These domains are located at nearly the same z-coordinate and are responsible for the flat appearance of this surface when viewed from the side (Fig. 6 *c*), and they also define most of the boundaries of the large peripheral cavities on the top surface of the CRC (Fig. 6 *a*). The flatness of the CRC's top surface is not an artifact caused by interactions of this surface with the carbon support film of the electron microscope grid (or any other interface) because side views of the CRC, both of isolated channels and channels reconstituted into lipid vesicles (Wagenknecht, T., J. Berkowitz, and R. Grassucci, unpublished results), also appear flat on this surface. Since domains 4, 5, and 6 would lie nearest the transverse tubule, it would seem that one or more of these domains are likely sites of interaction with transverse tubule components. Interestingly, the centers of the four clusters of domains 4–6 on the surface of the CRC are spaced 13.5-nm apart, just the spacing required to interact with the transverse tubule components identified by Block et al. (1988).

Communication between the Cytoplasmic and Transmembrane Assemblies

Considerable evidence argues that ligand-induced structural changes in the cytoplasmic assembly affect channel activity in the transmembrane domain. In excitation-contraction coupling, changes in the polarization of the transverse tubule membrane must somehow be communicated across the triad junction to the CRC in the apposing junctional face membrane of the SR. Most of the gap between the two membrane systems is bridged by the cytoplasmic assembly of the CRC and it seems likely that it must mediate signal transduction. In skeletal muscle, a direct interaction between the dihydropyridine receptor and the CRC cytoplasmic assembly is thought to exist through which depolarization-induced structural changes in the dihydropyridine receptor induce structural changes in the cytoplasmic assembly of the CRC which, in turn, potentiate channel gating.

From analysis of the sequence of the CRC, several potential regulatory sites have been proposed to lie in regions of the sequence thought to form the cytoplasmic assembly (Zorzato et al., 1990). Binding of calmodulin, a known modulator of the CRC, to the cytoplasmic assembly at a site remote from the transmembrane assembly (*at or near the cleft* between domains 4 and 6) has been observed in our laboratory by electron microscopy (Wagenknecht et al., 1994).

It appears, on the basis of our three-dimensional reconstructions, that the communication between the cytoplasmic and transmembrane assemblies implied by the above studies must be mediated by domain 1 (see Fig. 7), which forms the only visible physical link between the two. Perhaps the most intriguing structural feature of the reconstruction is the plug-like mass of density that lies in the cytoplasmic mouth of the putative transmembrane channel (Fig. 7 *a*). This plug is close to, and quite possibly in direct contact with, the four copies of domain 1. We speculate that channel gating occurs through movements of, or structural changes within, the plug structure, and furthermore, that these transitions are produced by changes in the configuration of domain(s) 1 caused by allosteric binding of ligands at remote sites on the cytoplasmic assembly. Further electron microscopy studies of the CRC in defined structural states and at higher resolutions should allow these ideas to be tested.

This work was supported by the National Institutes of Health (AR40615 [T. Wagenknecht] and HL32711 [S. Fleischer]).

Received for publication 10 June 1994 and in revised form 18 July 1994.

References

Block, B. A., T. Imagawa, K. P. Campbell, and C. Franzini-Armstrong. 1988. Structural evidence for direct interaction between the molecular components of the transverse tubule/sarcoplasmic reticulum junction in skeletal muscle. *J. Cell Biol.* 107:2587–2600.

Booy, F. P., and J. B. Pawley. 1993. Cryo-crinkling—what happens to carbon films on copper grids at low temperature. *Ultramicroscopy.* 48:273–280.

Brillantes, A.-M., K. Ondrias, A. Scott, E. Kobrinsky, E. Ondriasova, M. C. Moschella, T. Jayaraman, M. Landers, B. E. Ehrlich, and A. R. Marks. 1994. Stabilization of calcium release channel (ryanodine receptor) function by FK506-binding protein. *Cell.* 77:513–523.

Carazo, J. M. 1992. The fidelity of 3D reconstructions from incomplete data and the use of restoration methods. *In* Electron Tomography. J. Frank, editor. Plenum Press, New York. 117–166.

Carazo, J. M., and J. L. Carrascosa. 1987*a*. Restoration of direct Fourier three-dimensional reconstructions of crystalline specimens by the method of convex projections. *J. Microsc.* 145:159–177.

Carazo, J. M., and J. L. Carrascosa. 1987*b*. Information recovery in missing angular data cases: an approach by the convex projections method in three dimensions. *J. Microsc.* 145:23–43.

Caswell, A. H., and N. R. Brandt. 1989. Does muscle activation occur by direct mechanical coupling of transverse tubules to sarcoplasmic reticulum? *Trends. Biochem. Sci.* 14:161–165.

Caswell, A. H., N. R. Brandt, J.-P. Brunschwig, and S. Purkerson. 1991. Localization and partial characterization of the oligomeric disulfide-linked molecular weight 95,000 protein (triadin) which binds the ryanodine and dihydropyridine receptors in skeletal muscle triadic vesicles. *Biochemistry.* 30:7507–7513.

Catterall, W. A. 1991. Excitation-contraction coupling in vertebrate skeletal muscle: a tale of two calcium channels. *Cell.* 64:871–874.

Chiu, W. 1993. What does electron cryomicroscopy provide that X-ray crystallography and NMR spectroscopy cannot. *Annu. Rev. Biophys. Biomol. Struct.* 22:233–255.

Cyrklaff, M., M. Adrian, and J. Dubochet. 1990. Evaporation during preparation of unsupported thin vitrified aqueous layers for cryo-electron microscopy. *J. Electron Microsc. Tech.* 16:351–355.

Downing, K. H., and R. M. Glaeser. 1986. Improvement in high resolution image quality of radiation-sensitive specimens achieved with reduced spot size of the electron beam. *Ultramicroscopy.* 20:269–278.

Ferguson, D. G., H. W. Schwartz, and C. Franzini-Armstrong. 1984. Subunit structure of junctional feet in triads of skeletal muscle: a freeze-drying, rotary-shadowing study. *J. Cell Biol.* 99:1735–1742.

Fleischer, S., and M. Inui. 1989. Biochemistry and biophysics of excitation-contraction coupling. *Annu. Rev. Biophys. Biophys. Chem.* 18:333–364.

Frank, J. 1990. Classification of macromolecular assemblies studied as 'single particles'. *Quart. Rev. Biophys.* 23:281–329.

Frank, J., and M. van Heel. 1982. Correspondence analysis of aligned images of biological particles. *J. Mol. Biol.* 161:134–137.

Frank, J., and A. Verschoor. 1984. Masks for prescreening of molecule projections. *J. Mol. Biol.* 178:696–698.

Frank, J., and M. Radermacher. 1992. 3-Dimensional reconstruction of single particles negatively stained or in vitreous ice. *Ultramicroscopy.* 46:241–262.

Frank, J., B. Shimkin, and H. Dowse. 1981*a*. SPIDER-a modular software system for electron image processing. *Ultramicroscopy.* 6:343–358.

Frank, J., A. Verschoor, and M. Boublik. 1981*b*. Computer averaging of electron micrographs of 40S ribosomal subunits. *Science (Wash. DC).* 214: 1353–1355.

Frank, J., J. P. Bretaudiere, J. M. Carazo, A. Verschoor, T. Wagenknecht. 1988. Classification of images of biomolecular assemblies: a study of ribosomes and ribosomal subunits of Escherichia coli. *J. Microsc.* 150:99–115.

Franzini-Armstrong, C. 1980. Structure of the sarcoplasmic reticulum. *Fed. Proc.* 39:2403–2409.

Franzini-Armstrong, C., and G. Nunzi. 1983. Junctional feet and particles in the triads of a fast-twitch muscle fibre. *J. Muscle Res. Cell Motil.* 4:233–252.

Gerchberg, R. W. 1974. Super-resolution through error energy reduction. *Optica Acta.* 21:709–720.

Gerchberg, R. W., and W. O. Saxton. 1973. Wave phase from image and diffraction plane pictures. *In* Image Processing and Computer-aided Design in Electron Optics. P. W. Hawkes, editor. Academic Press, New York. 66–81.

Glaeser, R. M. 1992. Specimen flatness of thin crystalline arrays – influence of the substrate. *Ultramicroscopy.* 46:33–43.

Hymel, L., M. Inui, S. Fleischer, and H. Schindler. 1988. Purified ryanodine receptor of skeletal muscle sarcoplasmic reticulum forms Ca^{2+}-activated oligomeric Ca^{2+} channels in planar bilayers. *Proc. Natl. Acad. Sci. USA.* 85:441–445.

Imagawa, T., J. S. Smith, R. Coronado, and K. P. Campbell. 1987. Purified ryanodine receptor from skeletal muscle sarcoplasmic reticulum is the Ca^{2+}-permeable pore of the calcium release channel. *J. Biol. Chem.* 252:16636–16643.

Inui, M., A. Saito, and S. Fleischer. 1987. Purification of the ryanodine receptor and identity with feet structures of junctional terminal cisternae of sarcoplasmic reticulum from fast skeletal muscle. *J. Biol. Chem.* 262:1740–1747.

Jayaraman, T., A.-M. Brillantes, A. P. Timerman, S. Fleischer, H. Erdjument-Bromage, P. Tempst, and A. P. Marks. 1992. FK-506 binding protein associated with the calcium release channel (ryanodine receptor). *J. Biol. Chem.* 267:9474–9477.

Lai, F. A., H. P. Erickson, E. Rousseau, Q. Y. Liu, and G. Meissner. 1988. Purification and reconstitution of the calcium release channel from skeletal muscle. *Nature (Lond.).* 331:315–319.

Lu, X., L. Xu, and G. Meissner. 1994. Activation of the skeletal muscle calcium release channel by a cytoplasmic loop of the dihydropyridine receptor. *J. Biol. Chem.* 269:6511–6516.

Marty, I., M. Robert, M. Villaz, K. De Jongh, L. Lai, W. A. Catterall, and M. Ronjat. 1994. Biochemical evidence for a complex involving dihydropyridine receptor and ryanodine receptor in triad junctions of skeletal muscle. *Proc. Natl. Acad. Sci. USA.* 91:2270–2274.

McPherson, P. S., and K. P. Campbell. 1993. The ryanodine receptor/Ca^{2+} release channel. *J. Biol. Chem.* 268:13765–13768.

Numa, S., T. Tanabe, H. Takeshima, A. Mikami, T. Niidome, S. Nishimura, B. A. Adams, and K. G. Beam. 1990. Molecular insights into excitation-contraction coupling. *Cold Spring Harbor Symp. Quant. Biol.* 55:1–7.

Radermacher, M. 1988. Three-dimensional reconstruction of single particles from random and nonrandom tilt series. *J. Electr. Micr. Technique.* 9:359–394.

Radermacher, M., T. Wagenknecht, A. Verschoor, and J. Frank. 1987. Three-dimensional reconstruction from a single-exposure random conical tilt series applied to the 50S ribosomal subunit of Escherichia coli. *J. Microsc.* 146:113–136.

Radermacher, M., T. Wagenknecht, R. Grassucci, J. Frank, M. Inui, C. Chadwick, and S. Fleischer. 1992. Cryo-EM of the native structure of the calcium release channel/ ryanodine receptor from sarcoplasmic reticulum. *Biophys. J.* 61:936–940.

Rios, E., and G. Pizarro. 1991. Voltage sensors of excitation-contraction coupling in skeletal muscle. *Physiol. Rev.* 71:849–908.

Rios, E., G. Pizarro, and E. Stefani. 1992. Charge movement and the nature of signal transduction in skeletal muscle excitation-contraction coupling. *Annu. Rev. Physiol.* 54:109–133.

Saito, A., S. Seiler, A. Chu, and S. Fleischer. 1984. Preparation and morphology of sarcoplasmic reticulum terminal cisternae from rabbit skeletal muscle. *J. Cell Biol.* 99:875–885.

Saito, A., M. Inui, M. Radermacher, J. Frank, and S. Fleischer. 1988. Ultrastructure of the calcium release channel of sarcoplasmic reticulum. *J. Cell Biol.* 107:211–219.

Saxton, W. O., and W. Baumeister. 1982. The correlation averaging of a regularly arranged bacterial envelope protein. *J. Microsc.* 127:127–138.

Sezan, M. I., and H. Stark. 1982. Image restoration by the methods of convex projections. II Applications and numerical results. *IEEE Trans. Med. Imaging.* MI-1:95–101.

Sezan, M. I. 1992. An overview of convex projections theory and its application to image recovery problems. *Ultramicroscopy.* 40:55–67.

Smith, J. S., T. Imagawa, J. Ma, M. Fill, K. P. Campbell, and R. Coronado. 1988. Purified ryanodine receptor from rabbit skeletal muscle is the calcium-release channel of sarcoplasmic reticulum. *J. Gen. Physiol.* 92:1–26.

Speicher, D. W., and J. A. Ursitti. 1994. Conformation of a mammoth protein. *Curr. Biol.* 4:154–157.

Stewart, M., and G. Vigers. 1986. Electron microscopy of frozen-hydrated biological material. *Nature (Lond.).* 319:631–636.

Takeshima, H., S. Nishimura, T. Matsumoto, H. Ishida, N. Kangawa, N. Minamino, H. Matsuo, M. Ueda, M. Hanaoka, T. Hirose, and S. Numa. 1989. Primary structure and expression from complementary DNA of skeletal muscle ryanodine receptor. *Nature (Lond.).* 339:439–445.

Timerman, A. P., E. Ogunbumni, E. Freund, G. Wiederrecht, A. R. Marks, and S. Fleischer. 1993. The calcium release channel of sarcoplasmic reticulum is modulated by FK-506-binding protein. Dissociation and reconstitution of FKBP-12 to the calcium release channel of skeletal muscle sarcoplasmic reticulum. *J. Biol. Chem.* 268:22992–22999.

Unser, M., B. L. Trus, and A. C. Steven. 1987. A new resolution criterion based on spectral signal-to-noise ratios. *Ultramicroscopy.* 23:39–51.

van Heel, M., and J. Frank. 1981. Use of multivariate statistics in analyzing the images of biological macromolecules. *Ultramicroscopy.* 6:187–194.

van Heel, M., W. Keegstra, W. Schutter, E. J. F. van Bruggen. 1982. Arthropod hemocyanin structures studied by image analysis. *In* Life Chemistry Reports Suppl. 1. The structure and function of invertebrate respiratory proteins. E. J. Wood, editor. EMBO workshop, Leeds, UK. 69–73.

Wagenknecht, T., R. Grassucci, J. Frank, A. Saito, M. Inui, S. Fleischer. 1989. Three-dimensional architecture of the calcium channel/foot structure of sarcoplasmic reticulum. *Nature (Lond.).* 338:167–170.

Wagenknecht, T., J. Berkowitz, R. Grassucci, A. P. Timerman, and S. Fleischer. 1994. Localization of calmodulin binding sites on the skeletal muscle ryanodine receptor by electron microscopy. *Biophys. J.* In press.

Youla, D. C., and H. Webb. 1982. Image restoration by the method of convex projections. *IEEE Trans. Med. Imaging.* vol. MI-1, 81–95.

Zemlin, F. 1989. Dynamic focussing for recording images from tilted samples in small-spot scanning with a transmission electron microscope. *J. Electron. Microsc. Technique.* 11:251–257.

Zorzato, F., J. Fujii, K. Otsu, M. Phillips, N. M. Green, F. A. Lai, G. Meissner, D. H. MacLennan. 1990. Molecular cloning of cDNA encoding human and rabbit forms of the Ca^{2+} release channel (ryanodine receptor) of skeletal muscle sarcoplasmic reticulum. *J. Biol. Chem.* 265:2244–2256.